nature geoscience

Article

https://doi.org/10.1038/s41561-023-01212-4

Increased tropical South Pacific western boundary current transport over the past century

Received: 31 August 2022

Accepted: 23 May 2023

Published online: 26 June 2023

Check for updates

Wen-Hui Chen[1] ✉, Haojia Ren[1] ✉, John C. H. Chiang[2,3], You-Lin Wang[3,4], Ren-Yi Cai-Li[1], Yi-Chi Chen[1], Chuan-Chou Shen[1,5,6], Frederick W. Taylor[7], Thomas M. DeCarlo[8], Chau-Ron Wu[3,4], Horng-Sheng Mii[4] & Xingchen Tony Wang[9]

The wind-driven meridional overturning circulation between the tropical and subtropical oceans is important for regulating decadal-scale temperature fluctuations in the Pacific Ocean and globally. An acceleration of the overturning circulation can act to reduce global surface temperature as ocean stores more heat. The equatorward low-latitude western boundary current represents a key component of the meridional circulation cell in the Pacific and a major source of water mass for the Equatorial Undercurrent, yet long-term observations of its transport are scarce. Here we demonstrate that the $^{15}N/^{14}N$ ratio recorded by *Porites* spp. corals in the western tropical South Pacific is sensitive to the exchanges of water masses driven by the western boundary transport. Using a 94-year coral record from the Solomon Sea, we report that the $^{15}N/^{14}N$ ratio declined as the global surface temperature rose. The record suggests that the South Pacific western boundary current has strengthened in the past century, and it may have contributed to the reported strengthening of the Equatorial Undercurrent. In addition, the $^{15}N/^{14}N$ record shows strong decadal variability, indicative of weaker equatorial Pacific upwelling and stronger western boundary transport when the eastern equatorial Pacific is in the warm stage of the Pacific Decadal Oscillation.

Instrumental and palaeoclimate records over the past century and millennia show clear decadal climate variability in the tropical Pacific[1], which modulates the rate of global temperature change in response to the rising level of greenhouse gases in the atmosphere. For example, decadal surface cooling in the eastern equatorial Pacific may be responsible for the slowdown of global warming between the 1940s and 1970s and post-1998, weakening the anthropogenic warming trend during the past century[2,3]. Decadal variability in the tropical Pacific also modulates the behaviour and characteristics of the El Niño/Southern Oscillation (ENSO)[4].

Climate models suggest that the decadal variability in the tropical Pacific arises from oceanic processes involving the upper-ocean

[1]Department of Geosciences, National Taiwan University, Taipei, Taiwan. [2]Department of Geography, University of California, Berkeley, CA, USA. [3]Research Center for Environmental Changes, Academia Sinica, Taipei, Taiwan. [4]Department of Earth Sciences, National Taiwan Normal University, Taipei, Taiwan. [5]High-Precision Mass Spectrometry and Environment Change Laboratory (HISPEC), Department of Geosciences, National Taiwan University, Taipei, Taiwan. [6]Research Center for Future Earth, National Taiwan University, Taipei, Taiwan. [7]Institute for Geophysics, Jackson School of Geosciences, University of Texas at Austin, Austin, TX, USA. [8]College of Natural and Computational Sciences, Hawai'i Pacific University, Honolulu, HI, USA. [9]Department of Earth and Environmental Sciences, Boston College, Chestnut Hill, MA, USA. ✉e-mail: whchen890037@gmail.com; abbyren@ntu.edu.tw

https://doi.org/10.1038/s41561-023-01212-4

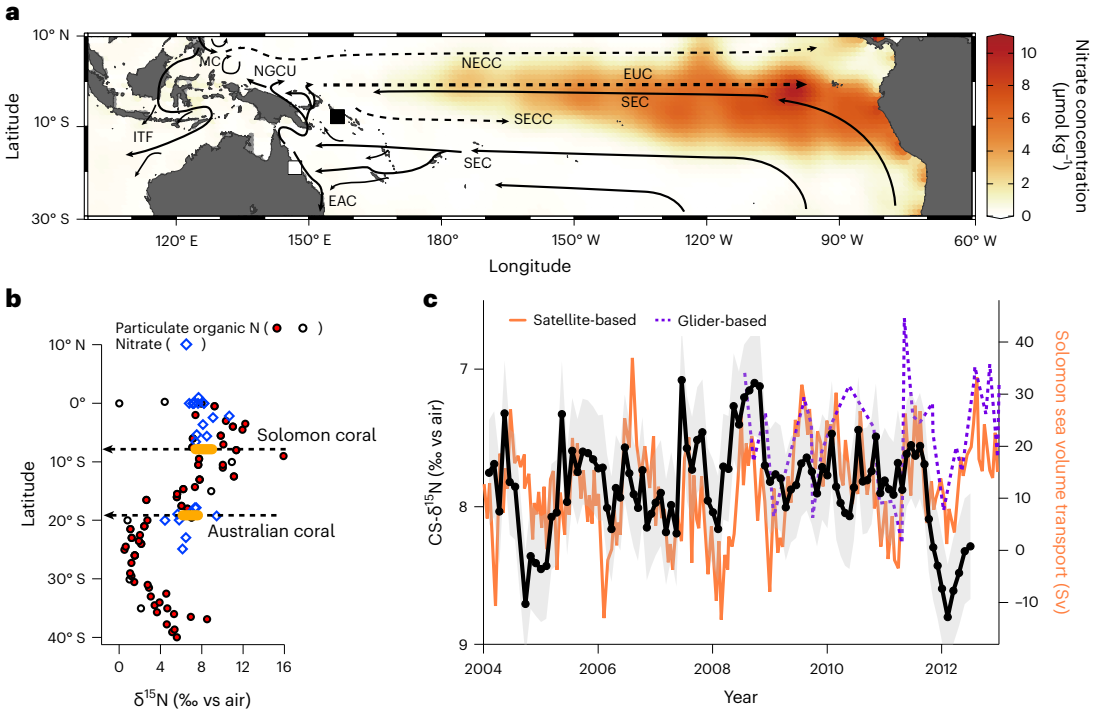

Fig. 1 | Coral skeletal nitrogen isotope variability in the Solomon Sea is determined by the inflow of subtropical water through the LLWBC transport. **a**, The map of annual mean surface ocean nitrate concentration (in micromole per kilogram) (ref. 48) in the tropical Pacific. Also plotted are the locations of the *Porites* coral core in this study from the Solomon Sea (filled square) and a published CS-δ^{15}N record from the Australian coast (open square). The major surface and subsurface currents are shown in solid and dashed arrows. The currents include North Equatorial Counter-Current (NECC), New Guinea Coastal Undercurrent (NGCU), EUC, South Equatorial Current (SEC), South Equatorial Counter-Current (SECC), Eastern Australian Current Indonesian Through-Flow (ITF) and Mindanao Current (MC)[49]. The map is generated with Ocean Data View[50]. **b**, The δ^{15}N of upper-ocean nitrate (concentration-weighted for the upper 300 m; blue diamonds[23,26,51,52]) and suspended particulate organic nitrogen (open circles from ref. 24; red circles from ref. 53) in the western tropical Pacific show a clear meridional gradient. The latitudes of the two coral cores are marked with the dashed arrows, and the range of their CS-δ^{15}N changes in the most recent decade are shown with the orange bars. **c**, CS-δ^{15}N (black points; grey shadings represent average 1σ of replicated samples for the whole record) is lower when the equatorward volume transport through the Solomon Sea is enhanced based on satellite and proxy derived (orange: 0–500 m (ref. 17)) and glider-based (violet: 0–700 m (refs. 16,54)) observations since 2004 (positive values indicate equatorward transport).

overturning circulation known as subtropical–tropical cells (STCs)[5–7]. The STCs are primarily driven by surface wind forcing[8]. Subduction of subtropical water in the eastern Pacific, which flows westward and equatorward in the upper pycnocline layers through both western boundary and interior pathways, feeds into the Equatorial Undercurrent and upwells into surface equatorial water before returning to the subtropics in the surface Ekman layer[8]. Observations suggest a slowdown of the interior transport since the end of the 1970s along with rapid warming of the eastern equatorial Pacific and globally[5], supporting the importance of the tropical–subtropical link in controlling tropical Pacific decadal variability. However, this remains very challenging to demonstrate observationally, owing to the insufficient instrumental record of oceanic processes.

The Solomon Sea in the western tropical South Pacific provides a western boundary connection between the subtropics and the Equator (Fig. 1a). The equatorward low-latitude western boundary current (LLWBC) transport through the Solomon Sea represents an important fraction of pycnocline transport in the meridional circulation cell[9] and a major source for the Equatorial Undercurrent (EUC)[10] that upwells along its eastward route and directly influences equatorial Pacific sea surface temperature[11,12]. The LLWBC transport in the surface layer of the Solomon Sea also contributes to the variability of the warm water volume (WWV), which has been suggested to impact ENSO dynamics[13]. As a result, changes in either the amount or properties of the water coming through the Solomon Sea have the potential to create global-scale feedbacks[5,14,15].

Glider-based observations of the Solomon circulation indicate that the equatorward flow is composed of both a tropical-wind-driven shallow flow ('tropical' mode) and the LLWBC transport that is probably forced remotely by subtropical winds ('subtropical' mode)[16,17]. During an El Niño, the reduced equatorial easterlies are associated with negative wind stress curl anomalies in the South Pacific. The decreased equatorial wind stress reduces the strength of the STCs, while the negative wind stress curl anomalies enhance the equatorward transport in the Solomon Sea, bringing more waters of subtropical origin towards the Equator[18]. On decadal and longer timescales, modelling results suggest that the strength of the Solomon Sea LLWBC transport is strongly correlated with the poleward transport in the interior, indicating a tendency for the LLWBC to compensate for the interior transport changes[6,19,20]. However, existing observational time series are not long enough to determine decadal variations in LLWBC transport.

Nitrogen isotopes as a proxy for LLWBC transport

The isotopic composition of marine nitrogen (N) and its temporal variations can help constrain the LLWBC transport in the Solomon Sea. In the western tropical Pacific (WTP), the ^{15}N/^{14}N ratio (or δ^{15}N) in both the upper thermocline nitrate (<400 m) and the near-surface suspended particulate organic nitrogen (PON) show clear tropical-to-subtropical changes on both sides of the Equator (Fig. 1b and Extended Data Fig. 1). The high δ^{15}N values close to the Equator in the WTP arise from processes associated with upwelling and productivity along the Equator. Easterly winds shoal the thermocline and drive upwelling of cool, nutrient-rich thermocline waters along the Equator and in the eastern margin of the basin, yet biological production in the upwelling regions is iron-limited[21]. As a result, the eastern and central equatorial Pacific

https://doi.org/10.1038/s41561-023-01212-4

(EEP and CEP) are characterized by incomplete consumption of the major nutrients (nitrate and phosphate), with substantial nutrient concentrations remaining in their surface waters (Fig. 1a) to be transported westward and poleward. When nitrate is consumed by phytoplankton, the lighter ^{14}N isotope is preferentially incorporated, causing the remaining nitrate pool (and thus also the PON subsequently produced from it) to become progressively enriched in the heavier ^{15}N isotope[22]. As a result, the $\delta^{15}N$ of the surface nitrate and the suspended PON is observed to increase from east to west[23,24]. The high $\delta^{15}N$ signal is also incorporated into sinking particles, the remineralization of which can elevate thermocline nitrate $\delta^{15}N$ on a regional basis[23,25] (Fig. 1b, Extended Data Fig. 1 and Supporting Information). As a result, although surface nitrate is exhausted, the high $\delta^{15}N$ propagates further into the WTP including the Solomon Sea by cycles of production and regeneration of PON (and possibly also dissolved organic N) that is elevated in $\delta^{15}N$ (refs. 24,25).

On the other hand, the subtropical waters flowing into the Solomon Sea have distinctively low $\delta^{15}N$ in the upper thermocline, due to the N input from regional N_2 fixation[26] (Fig. 1b and Extended Data Fig. 1). As a result, the $\delta^{15}N$ changes in the upper Solomon Sea water column can be strongly influenced by altering the relative proportion of equatorial vs subtropical waters on different timescales. During El Niño events or under an El Niño-like climate state, the intensification of the equatorward flow in the Solomon Sea would tend to lower the $\delta^{15}N$ in the upper ocean.

These subtropical waters are carried to the western boundary by the South Equatorial Current (SEC), which bifurcates in the Coral Sea at or before the coast of Australia, turning north into the Solomon Sea towards the Equator, and south into the East Australian Current (EAC) (Fig. 1a). Given the meridional $\delta^{15}N$ gradient, the western boundary currents would work to redistribute $\delta^{15}N$ anomalies northward towards the Equator and southward to the subtropical gyre. When the SEC intensifies, such as during and after an El Niño[27], it increases the equatorward transport to the Solomon Sea[28] and lowers the $\delta^{15}N$ in the upper ocean. In the meantime, it should also increase the southward transport along the Australian coast[28] and increases the $\delta^{15}N$ there. As a result, the $\delta^{15}N$ changes in the Solomon Sea should also have an opposing phasing with $\delta^{15}N$ changes along the Australian coast on various timescales.

Lacking seasonal-to-interannual-resolved nitrogen isotope measurements or sample collections in the Solomon Sea, we turn to a subseasonally resolved coral record from the Solomon Sea to test our hypothesis (Extended Data Fig. 2 and Methods). We also compare the Solomon Sea record with a published coral record in the Australian coast (19.15° S, 146.87° E)[29]. Scleractinian corals acquire their N from the environment, primarily by feeding on zooplankton and PON in surface waters under low-nutrient conditions in the WTP[30]. To facilitate the growth of coral skeleton, corals produce a small amount of organic material (for example, polysaccharide and proteins) in the extracellular calcifying medium, which is subsequently preserved in the mineral matrix[31]. The coral skeleton protects the organic matter against the diagenetic loss and exogenous N contamination that introduces uncertainty into non-fossil-bound archives of organic matter[32]. Thus, coral skeletal $\delta^{15}N$ (CS-$\delta^{15}N$) can record upper-ocean $\delta^{15}N$ changes in the WTP.

On seasonal timescales, the Solomon Sea CS-$\delta^{15}N$ changes in accordance with variations in the LLWBC transport estimated from glider data[16] and from satellite and proxy data[17] since 2004 (Fig. 1c). The CS-$\delta^{15}N$ is lower in austral winters when transport of cold and saline subtropical waters into the Solomon Sea is enhanced[33]. On interannual timescales, the Solomon Sea CS-$\delta^{15}N$ has a negative correlation with the temperature anomalies in the CEP and EEP, with lower CS-$\delta^{15}N$ when the surface of CEP and EEP are abnormally warm ($r = -0.50$, $P = 0.07$; the interannual variability in CS-$\delta^{15}N$ is defined by ensemble empirical mode decomposition or ensemble empirical mode decomposition (EEMD) analyses[34] and the Niño 3.4 index sea surface temperature

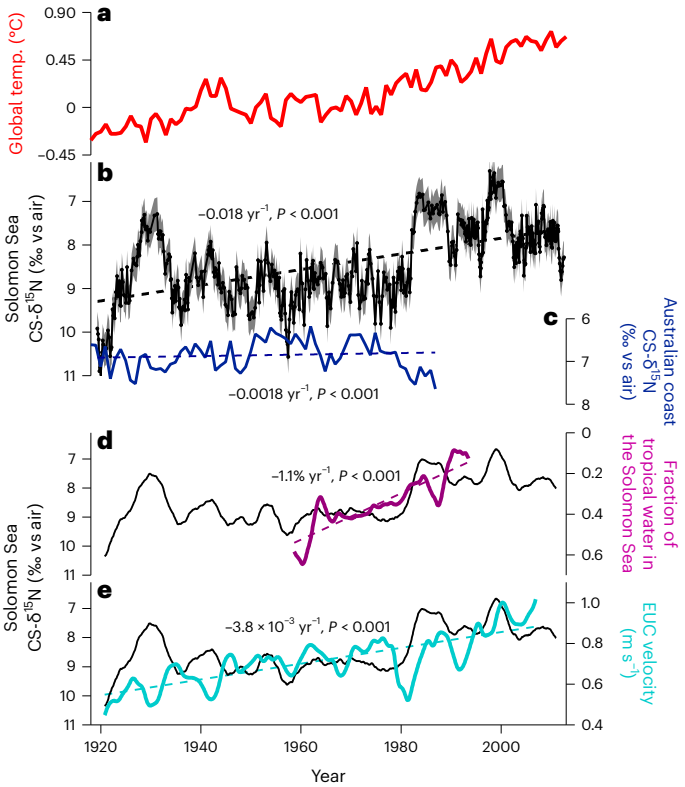

Fig. 2 | Long-term declines in the Solomon Sea coral skeletal nitrogen isotope ratios are associated with twenty-first century change in the climate and oceanic processes in the Pacific and globally. a, The rising trend of global surface temperature (temp.)[55]. **b**, The Solomon Sea CS-$\delta^{15}N$, with grey shadings representing the average 1σ of replicated samples. **c**, The published CS-$\delta^{15}N$ record from the Australian coast is relatively constant over this period[29]. **d**, Radiocarbon-based calculations of the fraction of eastern equatorial water in the upper Solomon Sea indicate a decline in tropical water in the Solomon Sea[38]. **e**, The EUC is shown to intensify over the last century (maximum EUC strength and zonal velocity at 0° N, 146° W and 112 m depth)[44]. Note that all the data series in **d** and **e** have been smoothed by a 3-year running mean.

(SST) anomaly is smoothed by 3-month running average; Methods). On decadal timescales, the Solomon Sea CS-$\delta^{15}N$ has a strong negative correlation with changes in the CS-$\delta^{15}N$ from the Australian coast with a negative phase ($r = -0.77$, $P = 0.01$, detrended and 7-year running average for both CS-$\delta^{15}N$ records) (Figs. 2 and 3; Methods). This evidence supports our hypothesis that the $\delta^{15}N$ dynamics in the WTP are regulated by basin-wide processes associated with the western boundary currents.

Over the past century, our CS-$\delta^{15}N$ record in the Solomon Sea is characterized by strong interannual and decadal changes superimposed on a long-term declining trend (Fig. 2b). In the following, we will discuss the decadal variability and long-term trend in the CS-$\delta^{15}N$ record before we return to the implications for tropical climate, that is, the ENSO cycles.

Decadal changes in the coral skeletal nitrogen isotope ratio

The variability in the Solomon Sea CS-$\delta^{15}N$ on decadal timescales is strongly correlated with basin-wide changes in the SST (Fig. 3d and Extended Data Fig. 3). In particular, the CS-$\delta^{15}N$ changes appear to be strongly correlated with the SST changes associated the Pacific Decadal Oscillation (PDO), which reflect the leading mode of climate variability in the Pacific on decadal timescales (Fig. 3d and Extended Data Fig. 3). The PDO manifests as a low-frequency El Niño-like pattern of climate variability with a warm tropical Pacific and weakened trade winds

https://doi.org/10.1038/s41561-023-01212-4

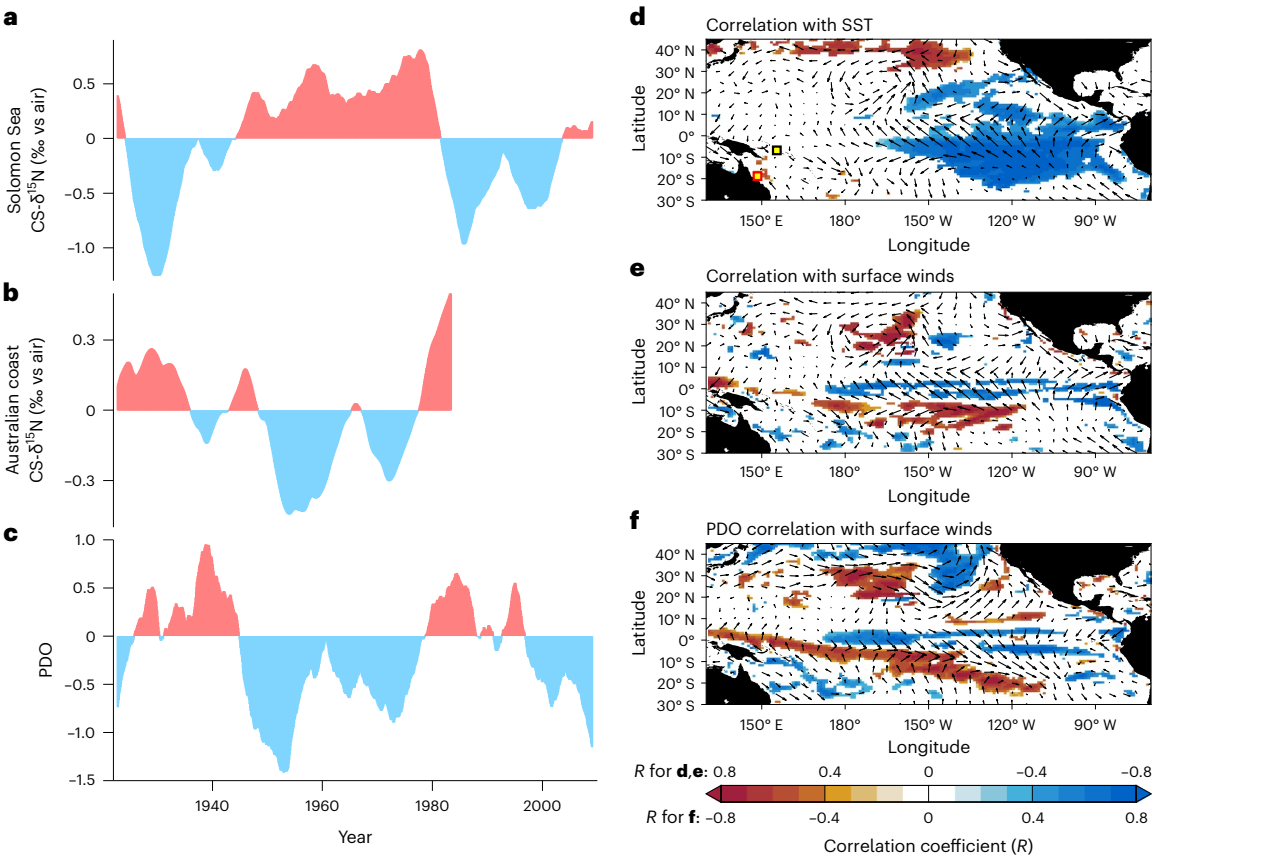

Fig. 3 | Decadal changes in the coral skeletal nitrogen isotope ratios are linked to Pacific Decadal Oscillation. a–**c**, The decadal changes in the Solomon Sea CS-δ^{15}N (**a**) are significantly correlated with the Australian coast CS-δ^{15}N (ref. 29) ($r = -0.77$, $P = 0.01$, 7-year running average; Methods) (**b**) and the PDO[56] ($r = -0.69$, $P = 0.03$, 10-year running average, with PDO leading by 46 months; Methods) (**c**). In **a**–**c**, positive and negative anomalies from the mean values are indicated with red and blue, respectively. **d**, Changes in the Solomon Sea CS-δ^{15}N are strongly correlated with basin-wide changes in the SST, especially with surface warming in the North Pacific, and surface cooling in the southeast Pacific. The locations of the Solomon Sea and Australian coast coral cores are shown in black and red squares. **e**,**f**, The Solomon Sea CS-δ^{15}N is also strongly correlated with the Pacific surface wind field (**e**) that is similar to the PDO-like wind patterns (**f**). On both **e** and **f**, vectors show correlation coefficient with wind stress, and shadings show correlation coefficient with wind stress curl (shading, above 90% confidence level; Methods). Note that the colour scales for **d** and **e** are the opposite from the colour scale for **f**. The long-term trend has been removed from the CS-δ^{15}N (ref. 29), and the 7-year running average has been applied before calculating the correlation. Maps in **d**–**f** were plotted using the MATLAB R2022 developed by MathWorks with 5 minute Gridded Global Relief Data (ETOPO5) from the National Geophysical Data Center (NGDC) of the National Oceanic and Atmospheric Administration (NOAA)[57]. The SST and wind are from Twentieth Century Reanalysis produced by the Earth System Research Laboratory Physical Sciences Division from NOAA and the University of Colorado Cooperative Institute for Research in Environmental Sciences (CIRES) using resources from Department of Energy (DOE) supercomputers (NOAA-20CR[58]): https://psl.noaa.gov/data/20thC_Rean/.

during its positive phase and a cool tropical Pacific and strengthened winds during its negative phase. The resemblance of the spatial pattern of our CS-δ^{15}N correlation with the SST to the PDO pattern is evidence that they are tied to similar wind changes that affect the wind-driven circulation in the southwestern Pacific. In support of this interpretation, the decadal changes in the Solomon Sea CS-δ^{15}N are significantly correlated with the whole Pacific wind field changes associated with PDO-like patterns (Fig. 3 and Extended Data Fig. 4) with changes in the North Pacific westerlies and wind stress curl in the Southeast Pacific. As a result, the overall decadal variations in the CS-δ^{15}N are significantly correlated with the PDO ($r = -0.69$, $P = 0.03$, 10-year running average; Methods) with 46 months lag (Extended Data Fig. 5).

On decadal timescales, the Solomon Sea CS-δ^{15}N is lower and the Australian coast CS-δ^{15}N is higher during positive PDO phases, consistent with basin-wide processes regulating the western boundary currents and redistributing the meridional δ^{15}N anomalies in the WTP (Figs. 2 and 3). The trade winds weaken during positive PDO phases, depressing Ekman divergence along the Equator and slowing down the pycnocline convergence in the interior[35,36]. In the meantime, the LLWBC intensifies due to enhanced Sverdrup transport driven by a negative wind stress curl anomaly between the weakened tropical trade winds and subtropical winds[19] (Fig. 3). CS-δ^{15}N changes in the Solomon Sea appear to lag behind changes in the tropical winds, especially since the 'climate regime shift' in 1976 (Extended Data Fig. 6), but are generally in phase with changes in the subtropical wind stress curl in the South Pacific (Extended Data Fig. 6). The overall correlation is strong between CS-δ^{15}N and wind stress curl in the South Pacific (Extended Data Fig. 6e) ($r = 0.52$, $P = 0.10$, with CS-δ^{15}N lagging by 9 months; Methods). These data thus suggest that the decadal variability in the equatorward LLWBC transport through the Solomon Sea, as inferred from the CS-δ^{15}N record, is remotely controlled by off-equatorial processes.

Assuming a simple linear wind-driven circulation, our data lends qualitative support for the modelling studies that demonstrate subtropical regulation of the STCs and the equatorial Pacific mean climate state[7]. The step-like decrease in CS-δ^{15}N in the early 1980s follows the observed thermocline shoaling in the WTP[37] (Extended Data Fig. 7b) and slowdown of the interior pycnocline transport[5]. These data together corroborate the view that variability in the STCs may contribute to decadal changes in the equatorial SST (Fig. 4).

https://doi.org/10.1038/s41561-023-01212-4

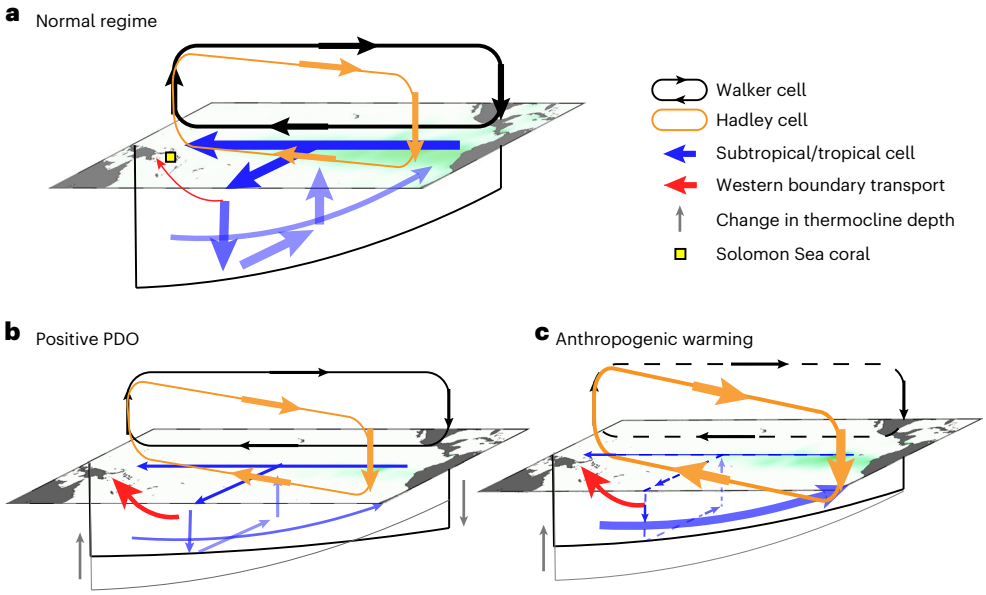

Fig. 4 | Schematic representation of the atmospheric and oceanic processes for different large-scale climate conditions that affect LLWBC transport. **a**, The STCs (blue arrows), Walker circulation (black arrows), Hadley circulation (orange arrows) and the LLWBC in the South Pacific (red arrow) are coupled processes. Green shadings represent the amount of nutrient upwelled and remaining at the surface of the CEP and EEP. **b**, The positive phase of the PDO is associated with a weaker Walker circulation, reduced equatorial winds and accompanied by weaker oceanic overturning circulation, flattened thermocline tilt and weaker upwelling in the CEP and EEP. The weaker trade winds, if not accompanied by changes in the subtropics, generate negative wind stress curl in the South Pacific, strengthening the LLWBC by Sverdrup transport. **c**, Schematic representation of projected changes associated with anthropogenic warming. Although the projected weakening in the Walker circulation and slowdown of the STCs are evident in most climate models, confidence in these projections is low (as indicated by dashed arrows) because of inconsistent signals in observations and model biases. Observations and models show a southward expansion of the Hadley cell and strengthening in the Southeasterly trade winds in the South Pacific[39], which would work to intensify the LLWBC transport[40] as suggested by the long-term decline in the Solomon Sea CS-δ^{15}N. Maps are generated with Ocean Data View[50].

Long-term decline in the Solomon Sea coral skeletal nitrogen isotope ratio

Underlying the interannual and interdecadal changes, CS-δ^{15}N has a long-term declining trend (−0.018 ‰ yr^{-1}, $p < 0.001$) that parallels the global warming trend (Fig. 2). The Australian coast CS-δ^{15}N indicates a relatively stable δ^{15}N in the subtropical South Pacific since the early twentieth century (Fig. 2c)[29], suggesting that the long-term decline in the Solomon CS-δ^{15}N cannot be explained by an overall decline in the subtropical δ^{15}N over the last century. Declines in the tropical δ^{15}N end member may result from reduced upwelling in the EEP and CEP, representing an 'El Niño-like' mean state change over the twenty-first century. However, the pattern of the observed ocean surface temperature trends since the 1950s is characterized by notable warming in the tropical western Pacific and Indian oceans and a slight cooling along the equatorial eastern Pacific, suggesting a 'La Niña-like' mean state change. This suggests that a long-term decline in the tropical δ^{15}N is unlikely to explain the Solomon CS-δ^{15}N change.

The long-term decline in the Solomon CS-δ^{15}N is best explained by an intensification of the LLWBC transport through the Solomon Sea. This is supported by radiocarbon-based evidence for increase of the subtropical waters in the Solomon Sea[38] (Fig. 2d). When the PDO returned to negative phase and the trade winds restrengthened in the late 1990s, the CS-δ^{15}N did not return to the high values of the previous negative PDO phase (1940–1980); this evidence suggests that processes other than the equatorial trade winds may be responsible for the long-term intensification of the LLWBC transport. Both models and historical data confirm a southward expansion of the southern edge of the Southern Hemisphere Hadley cell since 1979 (ref. 39). The associated intensification of the southeasterly trade winds and off-equatorial wind stress curl change in the South Pacific could enhance the LLWBC transport[40]. This mechanism is supported by the observed southward migration in the SEC bifurcation latitude[41] (Extended Data Fig. 7a) and an overall better correlation between CS-δ^{15}N and the wind stress curl in the South Pacific (Extended Data Fig. 6).

Because the waters from the Solomon Sea are the main source of the EUC[10,42,43], strengthening of the LLWBC transport inferred from our record would help to explain the observed long-term increase in the EUC transport[40,44] (Fig. 2e). This may then imply a growing importance of the LLWBC transport in regulating the water mass characteristics, heat/salt budget and climate dynamics in the equatorial Pacific and globally. In addition, recent works suggest that the LLWBC transport through the Solomon Sea is a major source of iron to the EUC[45], which eventually upwells and fuels productivity in the EEP. The strengthening in the LLWBC may then work to relieve iron limitation in the EEP in the future.

Implications for the tropical climate variability

We now return to discuss how LLWBC transport could contribute to the tropical climate variability dominated by the ENSO cycles on interannual timescales. While we anticipate enhanced LLWBC transport during and after an El Niño event, the data suggest a weakening relationship between ENSO activity and CS-δ^{15}N after the 1980s, caused by weakening correlation with La Niña conditions (Extended Data Fig. 8). We attempt to understand this nonlinear response to El Niño vs La Niña events with the 'recharge oscillator' model[13].

The model states that the depth of the mean thermocline, and hence the WWV above it, plays an important dynamical role in the ENSO cycle by controlling the temperature of the waters upwelled in the eastern equatorial Pacific, with a deeper mean thermocline resulting in the upwelling of warmer waters. As anthropogenic warming stratifies the upper ocean and shoals the mean thermocline along the Equator (Extended Data Fig. 7), upwelling of thermocline waters in the CEP and

EEP during La Niña conditions will more effectively strengthen the east–west temperature gradient, while El Niño conditions would require more WWV to be transported from the western Pacific warm pool[46]. On the one hand, periods of low LLWBC will become less important in raising the frequency of La Niña events. On the other hand, enhanced LLWBC transport would supply additional WWV, compensating for global warming's tendency to shoal the tropical thermocline, allowing the continued development of strong basin-wide El Niño events[47]. These two dynamics may explain the weakening relationship between ENSO and CS-δ^{15}N since the 1980s and imply growing importance of the LLWBC in modulating the tropical ENSO dynamics in the future.

Online content

Any methods, additional references, Nature Portfolio reporting summaries, source data, extended data, supplementary information, acknowledgements, peer review information; details of author contributions and competing interests; and statements of data and code availability are available at https://doi.org/10.1038/s41561-023-01212-4.

References

1. Power, S., Casey, T., Folland, C., Colman, A. & Mehta, V. Inter-decadal modulation of the impact of ENSO on Australia. *Clim. Dyn.* **15**, 319–324 (1999).
2. England, M. H. et al. Recent intensification of wind-driven circulation in the Pacific and the ongoing warming hiatus. *Nat. Clim. Change* **4**, 222–227 (2014).
3. Kosaka, Y. & Xie, S.-P. Recent global-warming hiatus tied to equatorial Pacific surface cooling. *Nature* **501**, 403–407 (2013).
4. Sun, T. & Okumura, Y. M. Impact of ENSO-like tropical Pacific decadal variability on the relative frequency of El Niño and La Niña events. *Geophys. Res. Lett.* **47**, e2019GL085832 (2020).
5. McPhaden, M. J. & Zhang, D. Slowdown of the meridional overturning circulation in the upper Pacific Ocean. *Nature* **415**, 603–608 (2002).
6. Capotondi, A., Alexander, M. A., Deser, C. & McPhaden, M. J. Anatomy and decadal evolution of the Pacific subtropical–tropical cells (STCs). *J. Clim.* **18**, 3739–3758 (2005).
7. Graffino, G., Farneti, R., Kucharski, F. & Molteni, F. The effect of wind stress anomalies and location in driving Pacific subtropical cells and tropical climate. *J. Clim.* **32**, 1641–1660 (2019).
8. McCreary, J. P. Jr & Lu, P. Interaction between the subtropical and equatorial ocean circulations: the subtropical cell. *J. Phys. Oceanogr.* **24**, 466–497 (1994).
9. Liu, Z. A simple model of the mass exchange between the subtropical and tropical ocean. *J. Phys. Oceanogr.* **24**, 1153–1165 (1994).
10. Tsuchiya, M., Lukas, R., Fine, R. A., Firing, E. & Lindstrom, E. Source waters of the Pacific equatorial undercurrent. *Prog. Oceanogr.* **23**, 101–147 (1989).
11. Qin, X., Sen Gupta, A. & van Sebille, E. Variability in the origins and pathways of Pacific Equatorial Undercurrent water. *J. Geophys. Res.: Oceans* **120**, 3113–3128 (2015).
12. Grenier, M. et al. From the western boundary currents to the Pacific Equatorial Undercurrent: modeled pathways and water mass evolutions. *J. Geophys. Res.: Oceans* **116**, C12044 (2011).
13. Jin, F.-F. An equatorial ocean recharge paradigm for ENSO. Part I: conceptual model. *J. Atmos. Sci.* **54**, 811–829 (1997).
14. Gu, D. & Philander, S. G. Interdecadal climate fluctuations that depend on exchanges between the tropics and extratropics. *Science* **275**, 805–807 (1997).
15. Kleeman, R., McCreary, J. P. Jr & Klinger, B. A. A mechanism for generating ENSO decadal variability. *Geophys. Res. Lett.* **26**, 1743–1746 (1999).
16. Kessler, W. S., Hristova, H. G. & Davis, R. E. Equatorward western boundary transport from the South Pacific: glider observations, dynamics and consequences. *Prog. Oceanogr.* **175**, 208–225 (2019).
17. Anutaliya, A. et al. Mooring and seafloor pressure end point measurements at the southern entrance of the Solomon Sea: subseasonal to interannual flow variability. *J. Geophys. Res.: Oceans* **124**, 5085–5104 (2019).
18. Davis, R. E., Kessler, W. S. & Sherman, J. T. Gliders measure western boundary current transport from the South Pacific to the equator. *J. Phys. Oceanogr.* **42**, 2001–2013 (2012).
19. Lee, T. & Fukumori, I. Interannual-to-decadal variations of tropical–subtropical exchange in the Pacific Ocean: boundary versus interior pycnocline transports. *J. Clim.* **16**, 4022–4042 (2003).
20. Lübbecke, J. F., Böning, C. W. & Biastoch, A. Variability in the subtropical–tropical cells and its effect on near-surface temperature of the equatorial Pacific: a model study. *Ocean Sci.* **4**, 73–88 (2008).
21. Coale, K. H. et al. A massive phytoplankton bloom induced by an ecosystem-scale iron fertilization experiment in the equatorial Pacific Ocean. *Nature* **383**, 495–501 (1996).
22. Sigman, D., Altabet, M., McCorkle, D., Francois, R. & Fischer, G. The δ^{15}N of nitrate in the Southern Ocean: consumption of nitrate in surface waters. *Glob. Biogeochem. Cycles* **13**, 1149–1166 (1999).
23. Rafter, P. A. & Sigman, D. M. Spatial distribution and temporal variation of nitrate nitrogen and oxygen isotopes in the upper equatorial Pacific Ocean. *Limnol. Oceanogr.* **61**, 14–31 (2016).
24. Horii, S., Takahashi, K., Shiozaki, T., Hashihama, F. & Furuya, K. Stable isotopic evidence for the differential contribution of diazotrophs to the epipelagic grazing food chain in the mid-Pacific Ocean. *Glob. Ecol. Biogeogr.* **27**, 1467–1480 (2018).
25. Lehmann, N. et al. Isotopic evidence for the evolution of subsurface nitrate in the Western Equatorial Pacific. *J. Geophys. Res.: Oceans* **123**, 1684–1707 (2018).
26. Knapp, A. N. et al. Distribution and rates of nitrogen fixation in the western tropical South Pacific Ocean constrained by nitrogen isotope budgets. *Biogeosciences* **15**, 2619–2628 (2018).
27. Kessler, W. S. & Cravatte, S. ENSO and short-term variability of the South Equatorial Current entering the Coral Sea. *J. Phys. Oceanogr.* **43**, 956–969 (2013).
28. Kessler, W. S. & Gourdeau, L. The annual cycle of circulation of the southwest subtropical Pacific, analyzed in an ocean GCM. *J. Phys. Oceanogr.* **37**, 1610–1627 (2007).
29. Erler, D. V. et al. Nitrogen isotopic composition of organic matter from a 168 year-old coral skeleton: implications for coastal nutrient cycling in the Great Barrier Reef Lagoon. *Earth Planet. Sci. Lett.* **434**, 161–170 (2016).
30. Wang, X. T. et al. Influence of open ocean nitrogen supply on the skeletal δ^{15}N of modern shallow-water scleractinian corals. *Earth Planet. Sci. Lett.* **441**, 125–132 (2016).
31. Drake, J. L. et al. How corals made rocks through the ages. *Glob. Change Biol.* **26**, 31–53 (2020).
32. Wang, X. T. et al. Deep-sea coral evidence for lower Southern Ocean surface nitrate concentrations during the last ice age. *Proc. Natl Acad. Sci. USA* **114**, 3352–3357 (2017).
33. Delcroix, T. et al. Sea surface temperature and salinity seasonal changes in the western Solomon and Bismarck seas. *J. Geophys. Res.: Oceans* **119**, 2642–2657 (2014).
34. Wu, Z. & Huang, N. E. Ensemble empirical mode decomposition: a noise-assisted data analysis method. *Adv. Adapt. Data Anal.* **1**, 1–41 (2009).
35. Meehl, G. A., Hu, A., Arblaster, J. M., Fasullo, J. & Trenberth, K. E. Externally forced and internally generated decadal climate variability associated with the Interdecadal Pacific Oscillation. *J. Clim.* **26**, 7298–7310 (2013).

36. Trenberth, K. E. & Fasullo, J. T. An apparent hiatus in global warming? *Earth's Future* **1**, 19–32 (2013).
37. Yang, H. & Wang, F. Revisiting the thermocline depth in the equatorial Pacific. *J. Clim.* **22**, 3856–3863 (2009).
38. Guilderson, T., Schrag, D. & Cane, M. Surface water mixing in the Solomon Sea as documented by a high-resolution coral ^{14}C record. *J. Clim.* **17**, 1147–1156 (2004).
39. Grise, K. M. et al. Recent tropical expansion: natural variability or forced response? *J. Clim.* **32**, 1551–1571 (2019).
40. Sen Gupta, A., Ganachaud, A., McGregor, S., Brown, J. N. & Muir, L. Drivers of the projected changes to the Pacific Ocean equatorial circulation. *Geophys. Res. Lett.* **39**, L09605 (2012).
41. Zhai, F., Hu, D., Wang, Q. & Wang, F. Long-term trend of Pacific South Equatorial Current bifurcation over 1950–2010. *Geophys. Res. Lett.* **41**, 3172–3180 (2014).
42. Blanke, B. & Raynaud, S. Kinematics of the Pacific Equatorial Undercurrent: an Eulerian and Lagrangian approach from GCM results. *J. Phys. Oceanogr.* **27**, 1038–1053 (1997).
43. Grenier, M. et al. From the subtropics to the central equatorial Pacific Ocean: neodymium isotopic composition and rare earth element concentration variations. *J. Geophys. Res.: Oceans* **118**, 592–618 (2013).
44. Drenkard, E. J. & Karnauskas, K. B. Strengthening of the Pacific equatorial undercurrent in the SODA reanalysis: mechanisms, ocean dynamics, and implications. *J. Clim.* **27**, 2405–2416 (2014).
45. Slemons, L. O., Murray, J. W., Resing, J., Paul, B. & Dutrieux, P. Western Pacific coastal sources of iron, manganese, and aluminum to the Equatorial Undercurrent. *Glob. Biogeochem. Cycles* **24**, GB3024 (2010).
46. Meinen, C. S. & McPhaden, M. J. Observations of warm water volume changes in the equatorial Pacific and their relationship to El Niño and La Niña. *J. Clim.* **13**, 3551–3559 (2000).
47. Meehl, G. A., Teng, H., Capotondi, A. & Hu, A. The role of interannual ENSO events in decadal timescale transitions of the Interdecadal Pacific Oscillation. *Clim. Dyn.* **57**, 1933–1951 (2021).
48. Boyer, T. P. et al. *World Ocean Atlas 2018* (NOAA National Centers for Environmental Information, 2018).
49. Schott, F. A., Wang, W. & Stammer, D. Variability of Pacific subtropical cells in the 50-year ECCO assimilation. *Geophys. Res. Lett.* **34**, L05604 (2007).
50. Schlitzer, R. Ocean data view. *Alfred Wegener Institute* https://odv.awi.de (2018).
51. Yoshikawa, C., Yamanaka, Y. & Nakatsuka, T. Nitrate-nitrogen isotopic patterns in surface waters of the western and central equatorial pacific. *J. Oceanogr.* **62**, 511–525 (2006).
52. Yoshikawa, C. et al. Nitrogen isotope ratios of nitrate and N* anomalies in the subtropical South Pacific. *Geochem. Geophys. Geosyst.* **16**, 1439–1448 (2015).
53. Raes, E. J. et al. N_2 fixation and new insights into nitrification from the ice-edge to the equator in the South Pacific Ocean. *Front. Mar. Sci.* **7**, 389 (2020).
54. Kessler, W. S. & Hristova, H. G. *Solomon Sea Volume Transport Time-Series Measured by Glider* (Scripps Institution of Oceanography, Instrument Development Group, 2019); https://doi.org/10.21238/S8SPRAY2718A
55. National Centers for Environmental Information *Climate at a Glance: Global Time Series* (NOAA, 2022).
56. Mantua, N. *The Pacific Decadal Oscillation. A Brief Overview for Non-specialists, to Appear in the Encyclopedia of Environmental Change* (Joint Institute for the Study of the Atmosphere and Oceans, Univ. of Washington, 1999).
57. National Geophysical Data Center *5-Minute Gridded Global Relief Data (ETOPO5)* (NOAA, 1993); https://doi.org/10.7289/V5D798BF
58. Slivinski, L. C. et al. Towards a more reliable historical reanalysis: improvements for version 3 of the twentieth century reanalysis system. *Q. J. R. Meteorolog. Soc.* **145**, 2876–2908 (2019).

Publisher's note Springer Nature remains neutral with regard to jurisdictional claims in published maps and institutional affiliations.

Open Access This article is licensed under a Creative Commons Attribution 4.0 International License, which permits use, sharing, adaptation, distribution and reproduction in any medium or format, as long as you give appropriate credit to the original author(s) and the source, provide a link to the Creative Commons license, and indicate if changes were made. The images or other third party material in this article are included in the article's Creative Commons license, unless indicated otherwise in a credit line to the material. If material is not included in the article's Creative Commons license and your intended use is not permitted by statutory regulation or exceeds the permitted use, you will need to obtain permission directly from the copyright holder. To view a copy of this license, visit http://creativecommons.org/licenses/by/4.0/.

© The Author(s) 2023

Methods

Coral core and age model

The coral core (12NAK-K) was drilled from a live *Porites* at 1 m water depth in August 2012 in the western Solomon Islands between Vella Lavella Island and Ranongga Island (7° 52′ 52.83″ S, 156° 30′ 14.61″ E). The site is remote and not close to major freshwater input. The core was subsequently sliced and stored at the University of Texas at Austin. One slice was sent to National Taiwan University for subsequent analyses. The coral core was passed through the Philips Ingenuity computed tomography (CT) scanner at Taiwan Instrument Research Institute. The coral skeletal density was determined from the CT scans[59] and is used to mark annual growth layers and derive the initial age model with annual resolution (Extended Data Fig. 2a). The average annual extension rate of this *Porites* coral is 1.3 cm yr^{-1}. We did not observe any distinct anomalously high-density bands that could be indicative of past bleaching events. Because the density bands are not clear before 1918 AD, we did not sample the materials before 1918 AD. We also used the CT scan to identify the axis of primary growth for subsampling (for example, red squares in Extended Data Fig. 2a). Subsamples were cut with a customized automated sawing machine along the primary growth axis. Each sample is 1 mm parallel to the growth axis, 11 mm perpendicular to the growth axis and 2 mm deep. Given the average extension rate, our sampling resolution is approximately 0.9 month. Each sample is collected into a centrifuge tube and gently ground with a pestle. Approximately 0.5–1 mg material from each sample is collected for carbonate $\delta^{18}O$ and $\delta^{13}C$ analyses, while the remaining material is stored for CS-$\delta^{15}N$ analyses. $\delta^{18}O$ is a measure of the ratio of oxygen stable isotopes ^{18}O and ^{16}O with respect to the the reference standard, Vienna Pee Dee Belemnite (VPDB). $\delta^{13}C$ is a measure of the ratio of carbon stable isotopes ^{13}C and ^{12}C with respect to VPDB. Both are expressed in δ notations. We first derive the CT-based annually resolved age model (CT age), then fine tune the age model by correlating annual cycles of $\delta^{18}O$ and $\delta^{13}C$ with satellite-observed SST (8° S, 156 °E, NOAA Extended Reconstructed Sea Surface Temperature (SST) V5, monthly resolution) (Extended Data Fig. 2b). The $\delta^{18}O$ is generally less negative during austral winters when the surface waters in the Solomon Sea are cold and saline[33], and $\delta^{13}C$ generally has higher values during austral summers, probably due to the increase in the $\delta^{13}C$ of the dissolved inorganic carbon (DIC) in the coral reef as a result of greater productivities in the warm seasons[60]. The relatively large sampling size could result in some time averaging across months, so we focus on discussing interannual, decadal and long-term changes in the CS-$\delta^{15}N$.

Analytical methods

Sample preparation and analyses for CS-$\delta^{15}N$ are all performed at Ren lab, Department of Geosciences, National Taiwan University. The protocol follows and is modified from that of ref. 61. First, in an oxidative cleaning step to remove external/contaminant organic matter, 8 ml of persulfate oxidizing reagent (POR) is added to ~20 mg of coral powder in 12 ml glass vials and autoclaved at 121 °C for 1 h. The cleaning reagent is decanted, and the sample is rinsed with Milli-Q water five times and then dried in a 60 °C oven. Once dry, cleaned coral (~7 mg per sample) is weighed into a 4 ml borosilicate glass vial (precombusted for 5 h at 500 °C) and dissolved in 0.65 µl of 4 N HCl. To each vial, 1 ml purified basic potassium POR is added, and the vials are then autoclaved for 1 h on a slow-vent setting to completely oxidize to nitrate the organic nitrogen released during decalcification. To lower the N blank associated with the oxidizing solution, the potassium persulfate is recrystallized four times. At the time of processing, 1.3 g NaOH and 0.5 g potassium persulfate are dissolved in 100 ml of Milli-Q water. Organic standards are used to constrain the $\delta^{15}N$ of the persulfate reagent blank. We use two organic standards: United States Geological Survey (USGS) 40 ($\delta^{15}N$ = −4.5‰ vs air) and a self-made mixture of 6-aminocaproic acid and glycine ($\delta^{15}N$ = 5.4‰ vs air). A minimum of eight organic standards and three to five blanks are analysed per batch of samples.

After oxidation, the sample is centrifuged, the clear supernatant is transferred to another precombusted 4 ml borosilicate glass vial, and the pH of the supernatant is adjusted to between 4 to 7 with HCl and NaOH. To determine the N content of the samples, we measure nitrate concentration in the oxidation solutions after autoclaving. Nitrate concentration is analysed by reduction to nitric oxide using vanadium(III) followed by chemiluminescence detection[62]. The N blank is also quantified in this way. Consistent with previous findings, *Porites* corals have an average N content of 2.3 µmol N per gram of clean aragonite, yielding nitrate concentrations in the oxidation solutions of ~15 µM, whereas the blank concentration ranges between 0.15 and 0.4 µM (less than 3%, typically less than 1%, of the total N per sample).

The $\delta^{15}N$ of the samples is determined using the denitrifier method in conjunction with gas chromatography and isotope ratio mass spectrometry[63]. The denitrifier method involves the transformation of dissolved nitrate and nitrite into nitrous oxide gas (N_2O) via a naturally occurring denitrifying bacterial strain that lacks an active form of the enzyme N_2O reductase. The denitrifier *Pseudomonas chlororaphis* was used for this work. Normally, 5 nmol sample amounts are added to 1.5 ml of bacterial concentrate after degassing of the bacteria. Along with the samples, the organic standards and replicate analyses of nitrate reference material IAEA-NO3 ($\delta^{15}N$ = 4.7‰ vs air), USGS-34 ($\delta^{15}N$ = −1.8‰ vs air) and a bacterial blank are also measured. We use the IAEA-NO3 and USGS-34 standards to monitor the bacterial conversion and the stability of the mass spectrometer, and we use the oxidation standards to correct for the oxidation blank. The denitrifier method typically has a standard deviation (1sd) of less than 0.1‰. An in-house coral standard provides a metric for repeatability both within an analysis batch and across batches, which indicates an analytical precision (1sd) of our protocol of 0.26‰.

Because of the slight changes in the extension direction of this coral, we divided the whole core into 13 parts for subsampling to subsample along the maximal growth axis. We collected ~10 subsamples overlapping in time from the adjacent parts for separate analyses. We use $\delta^{13}C$, $\delta^{18}O$ and CT image to correlate the overlapping samples and to combine these parts back into a complete record. In the same time, these samples can be considered as duplicate measurements on carbonate produced during the same time. The average 1sd (n = 87) of CS-$\delta^{15}N$ is 0.17‰ (from 0 to 0.64‰). This is probably an overestimation for our analytical error, given the uncertainties in the age when correlating the samples.

$\delta^{13}C$ and $\delta^{18}O$ are measured in the Department of Earth Sciences at the National Taiwan Normal University (NTNU) using a Micromass IsoPrime IRMS equipped with a Multicarb automatic system. The carbonate standard NBS-19 ($\delta^{13}C$ = 1.95‰, $\delta^{18}O$ = −2.20‰) is used to calibrate to Vienna Pee Dee Belemnite (VPDB). The average precisions of the NBS-19 are 0.04‰ and 0.05‰ for $\delta^{13}C$ and $\delta^{18}O$ (n = 115), respectively.

Correlation analyses. Each dataset is first smoothed with different methods described in the main text and detrended before calculating correlation between any two data series. To estimate the correlation significance level, the effective degree of freedom is calculated from the autocorrelation function[64].

Ethics statement

The conducted study considers diversity, equity and inclusion.

Data availability

Data are archived at NOAA National Centers for Environmental Information: https://www.ncei.noaa.gov/access/paleo-search/study/37698.

References

59. DeCarlo, T. M. Deriving coral skeletal density from computed tomography (CT): effects of scan and reconstruction settings. *Matters Select* **3**, e201706000005 (2017).

60. Swart, P. K., Leder, J., Szmant, A. & Dodge, R. The origin of variations in the isotopic record of scleractinian corals: II. carbon. *Geochim. Cosmochim. Acta* **60**, 2871–2885 (1996).
61. Ren, H. et al. 21st-century rise in anthropogenic nitrogen deposition on a remote coral reef. *Science* **356**, 749–752 (2017).
62. Braman, R. S. & Hendrix, S. A. Nanogram nitrite and nitrate determination in environmental and biological materials by vanadium(III) reduction with chemiluminescence detection. *Anal. Chem.* **61**, 2715–2718 (1989).
63. Weigand, M. A., Foriel, J., Barnett, B., Oleynik, S. & Sigman, D. M. Updates to instrumentation and protocols for isotopic analysis of nitrate by the denitrifier method. *Rapid Commun. Mass Spectrom.* **30**, 1365–1383 (2016).
64. Thomson, R. E. & Emery, W. J. *Data Analysis Methods in Physical Oceanography* (Newnes, 2014).
65. Huang, B. et al. Extended reconstructed sea surface temperature, version 5 (ERSSTv5): upgrades, validations, and intercomparisons. *J. Clim.* **30**, 8179–8205 (2017).
66. Rayner, N. et al. Global analyses of sea surface temperature, sea ice, and night marine air temperature since the late nineteenth century. *J. Geophys. Res.: Atmospheres* **108**, 4407 (2003).
67. Ebisuzaki, W. A method to estimate the statistical significance of a correlation when the data are serially correlated. *J. Clim.* **10**, 2147–2153 (1997).
68. Poli, P. et al. ERA-20C: an atmospheric reanalysis of the twentieth century. *J. Clim.* **29**, 4083–4097 (2016).
69. Dee, D. P. et al. The ERA-interim reanalysis: configuration and performance of the data assimilation system. *Q. J. R. Meteorolog. Soc.* **137**, 553–597 (2011).
70. Allan, R. & Ansell, T. A new globally complete monthly historical gridded mean sea level pressure dataset (HadSLP2): 1850–2004. *J. Clim.* **19**, 5816–5842 (2006).
71. Freeman, E. et al. ICOADS release 3.0: a major update to the historical marine climate record. *Int. J. Climatol.* **37**, 2211–2232 (2017).
72. Kalnay, E. et al. The NCEP/NCAR 40-year reanalysis project. *Bull. Am. Meteorolog. Soc.* **77**, 437–472 (1996).
73. Kanamitsu, M. et al. NCEP–DOE AMIP-II reanalysis (R-2). *Bull. Am. Meteorol. Soc.* **83**, 1631–1644 (2002).
74. Melet, A., Gourdeau, L., Verron, J. & Djath, B. Solomon Sea circulation and water mass modifications: response at ENSO timescales. *Ocean Dyn.* **63**, 1–19 (2013).
75. Kessler, W. S. Observations of long Rossby waves in the northern tropical Pacific. *J. Geophys. Res.: Oceans* **95**, 5183–5217 (1990).
76. Carton, J. A., Giese, B. S. & Grodsky, S. A. Sea level rise and the warming of the oceans in the Simple Ocean Data Assimilation (SODA) ocean reanalysis. *J. Geophys. Res.: Oceans* **110**, C09006 (2005).
77. Xu, K., Huang, R. X., Wang, W., Zhu, C. & Lu, R. Thermocline fluctuations in the equatorial Pacific related to the two types of El Niño events. *J. Clim.* **30**, 6611–6627 (2017).
78. Cheng, L. et al. Improved estimates of ocean heat content from 1960 to 2015. *Sci. Adv.* **3**, e1601545 (2017).

Acknowledgements

We are grateful for the work of A.K. Papabatu in obtaining the coral cores. We thank S.-Y. Yang for carbon and oxygen isotope analyses and J. Cotton for analyses of the CT images. Our work is inspired by conversations and discussions with D. Sigman, G. Burr and Y.-T. Hwang. This work is supported by Ministry of Science and Technology Taiwan, Columbus grant 111-2636-M-002-020- and 111-2116-M-032-MY3 (H.R.); Ministry of Science and Technology Taiwan, grant 110-2811-M-001-554 (J.C.H.C.); Ministry of Science and Technology Taiwan, grant 110-2611-M-003-001(C.-R.W., Y.-L.W.); Ministry of Science and Technology Taiwan, grant 110-2123-M-002-009 (C.-C.S.); US National Science Foundation, grant EAR-1119211 (F.W.T.); US National Science Foundation, grant OCE-2148926 (X.T.W.); and Ministry of Science and Technology Taiwan, grant 110-2116-M-003-005 (H.-S.M.). This is the University of Texas Institute for Geophysics (UTIG) publication #3958.

Author contributions

H.R. designed the study and interpreted the results. W.-H.C. processed coral samples and analysed CS-δ^{15}N. W.-H.C., H.R., J.C.H.C., C.-R.W., Y.-L.W. and R.-Y.C.-L. conducted data analyses. Y.-C.C., R.-Y.C.-L., C.-C.S. and X.T.W. provided technical assistance and training. T.M.D. and H.-S.M. constructed the age model. F.W.T. obtained the coral core from the Solomon Islands and provided coral materials. W.-H.C. and H.R. wrote the manuscript with contributions from all co-authors.

Competing interests

The authors declare no competing interests.

Additional information

Extended data is available for this paper at https://doi.org/10.1038/s41561-023-01212-4.

Supplementary information The online version contains supplementary material available at https://doi.org/10.1038/s41561-023-01212-4.

Correspondence and requests for materials should be addressed to Wen-Hui Chen or Haojia Ren.

Peer review information *Nature Geoscience* thanks William S. Kessler, Braddock Linsley and the other, anonymous, reviewer(s) for their contribution to the peer review of this work. Primary Handling Editor: James Super, in collaboration with the *Nature Geoscience* team.

Reprints and permissions information is available at www.nature.com/reprints.

https://doi.org/10.1038/s41561-023-01212-4

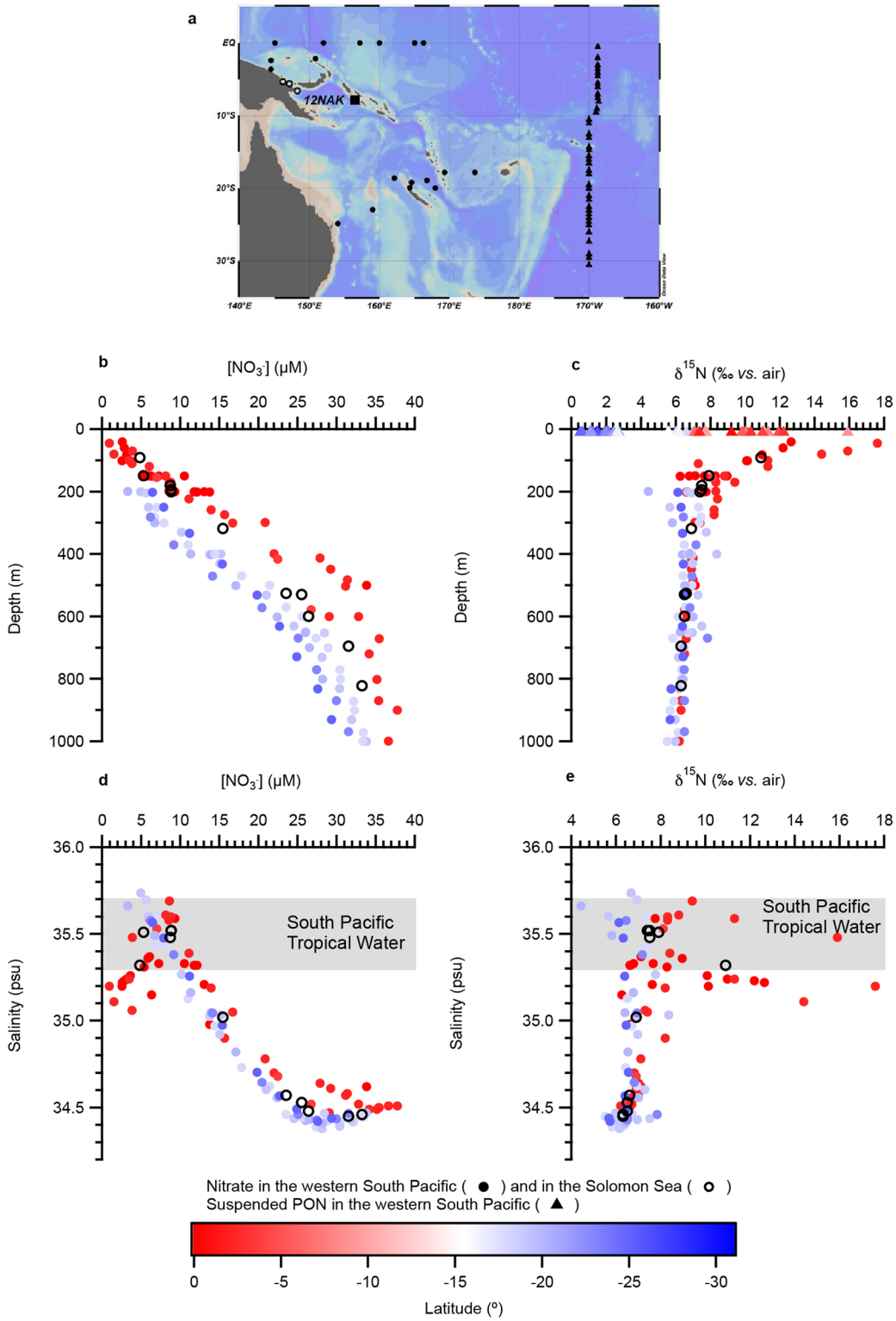

Extended Data Fig. 1 | Modern hydrography and $\delta^{15}N$ dynamics in the western tropical-subtropical South Pacific. a, Map of stations for nitrate depth profiles (circles; three stations in the Solomon Sea are marked with open circles) and for near surface (75 m) suspended particulate organic nitrogen (PON) (triangles). Location of the coral core is marked in square. **b**, Concentration of nitrate in the upper 1000 m. **c**, $\delta^{15}N$ of nitrate (circles) in the upper 1000 m and $\delta^{15}N$ suspended PON (triangles) at 75 m. Concentration and $\delta^{15}N$ of nitrate are plotted against salinity for the upper 1000 m from these stations (**d** and **e**). Data are from references[23,26,51,52]. Note that the $\delta^{15}N$ of nitrate for the South Pacific Tropical Water (SPTW) indicated by the high salinity are different in the tropical *vs.* subtropical stations. The subtropical SPTW has lower $\delta^{15}N$ due to remineralization of newly fixed nitrogen by N_2 fixation[52], whereas remineralization of suspended PON adds ^{15}N-enriched nitrate to the tropical thermocline at the southern edge of the equatorial Pacific upwelling[25]. In panels b–d, the colors indicate latitudes of the stations, except for the stations from the Solomon Sea, which are all shown with open black circles.

https://doi.org/10.1038/s41561-023-01212-4

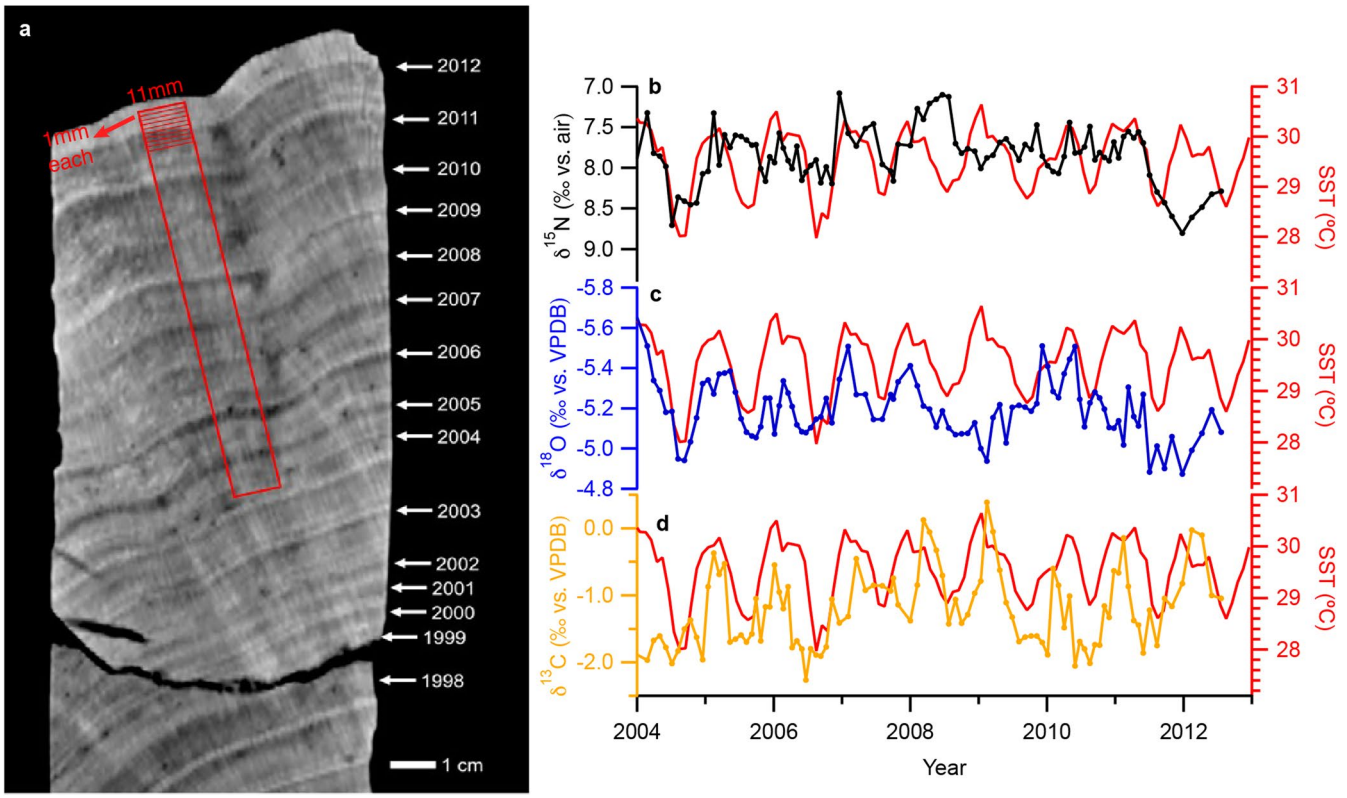

Extended Data Fig. 2 | Demonstration of age models based on CT and isotopes between 2004 and 2012. a, The coral skeletal density was determined from the CT scans[59], and is used to mark annual growth layers and derive the initial age model with annual resolution. The sampling line (red line) is chosen along its maximal growth direction. **b**-**d**, We then fine tune the age model by correlating $\delta^{18}O$ (panel **c**: blue) changes to satellite-observed SST (red) (8°S, 156°E, NOAA Extended Reconstructed Sea Surface Temperature (SST) V5, monthly resolution[65]).

https://doi.org/10.1038/s41561-023-01212-4

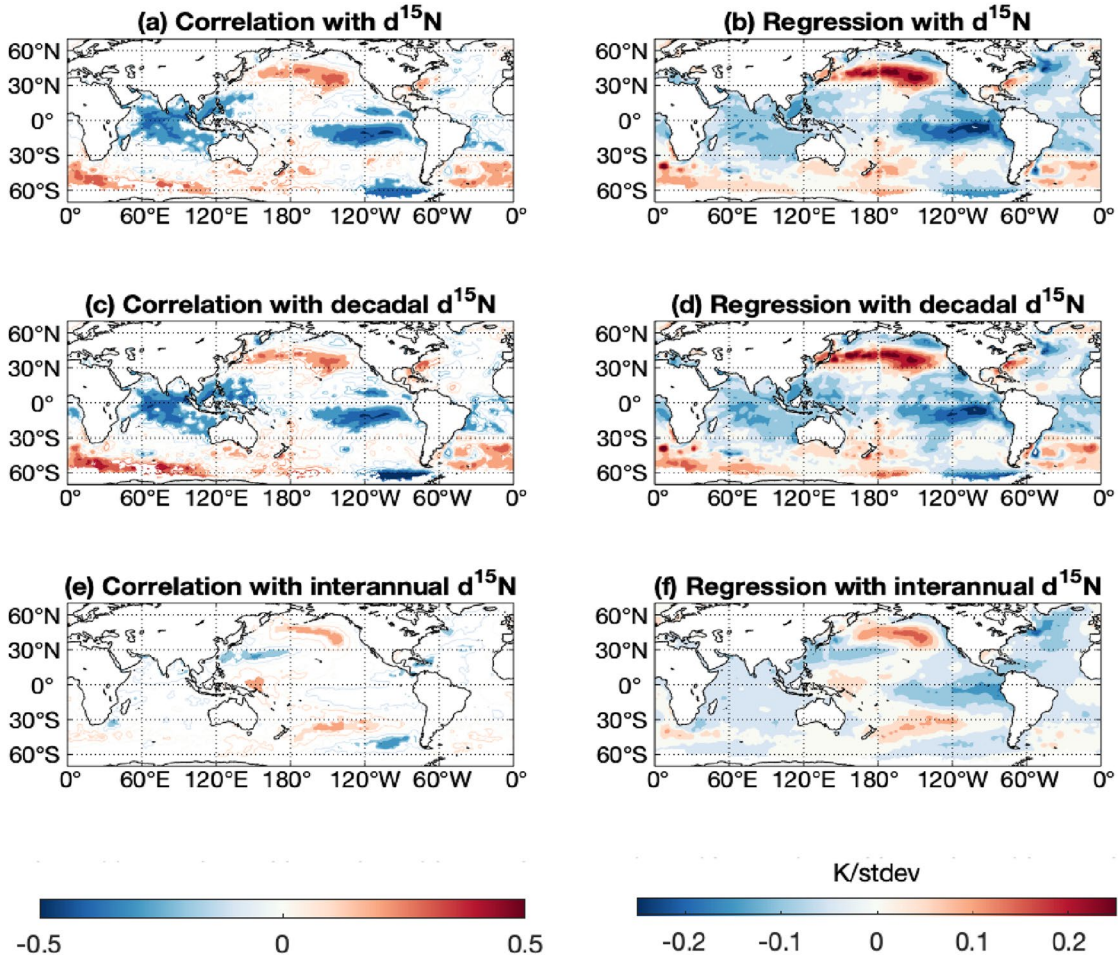

Extended Data Fig. 3 | Correlation (left panels) and regression (right panels) between changes in the CS-δ^{15}N and sea surface temperature. The overall decadal plus interannual changes (**a** and **b**), the decadal-only changes (**c** and **d**), and the interannual-only changes (**e** and **f**) of the CS-δ^{15}N, are all positively correlated with SST in the North Pacific, and negatively correlated with SST in the Southeast Pacific, a pattern that is led by Pacific Decadal Oscillation. Interannual and decadal variability in the CS-δ^{15}N are defined by the EEMD. Monthly anomalies in the CS-δ^{15}N were computed by removing the climatological monthly average from the data, and then detrended prior to conducting the correlation. The SST data is from the Hadley Centre Sea Ice and Sea Surface Temperature Dataset (HadISST) from 1919 to 2011 (ref. 66) (https://www.metoffice.gov.uk/hadobs/hadisst/). Contour interval for the correlation plot is 0.1, and regions where the correlation is significant ($p < 0.05$) are shaded. The contour interval for the regression is 0.05 K/stdev or K per standard deviation of the detrended CS-δ^{15}N time series. Significance of correlations is assessed using the t-statistic and with the effective sample size calculated using Equation 2 of ref. 67.

https://doi.org/10.1038/s41561-023-01212-4

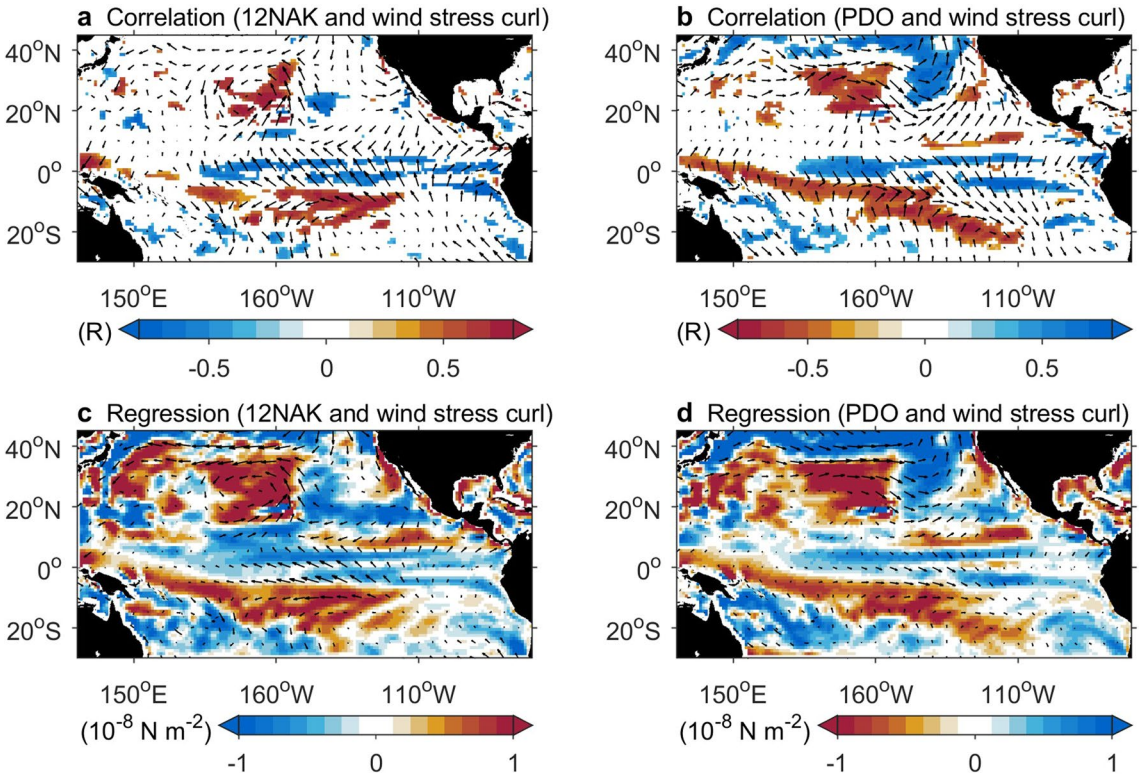

Extended Data Fig. 4 | Correlation between CS-δ^{15}N and Pacific wind field, in comparison with the wind field changes associated with PDO. a, Spatial pattern of the correlation coefficient between wind stress and the Solomon Sea CS-δ^{15}N (vector), and between wind stress curl and CS-δ^{15}N (shading, above 90% confidence level). To estimate the correlation significance level, the effective degree of freedom is calculated from the autocorrelation function[64]. **b** same as a, but is the result of PDO. **c** same as a, but is the result of regression coefficient between winds and CS-δ^{15}N. **d** same as c, but is the result of PDO. The long-term trend has been removed, and the 7-yr running average has been applied before calculating the correlation. The SST and wind are from NOAA-CIRES-DOE Twentieth Century Reanalysis (NOAA-20CR[58]). https://psl.noaa.gov/data/20thC_Rean/.

https://doi.org/10.1038/s41561-023-01212-4

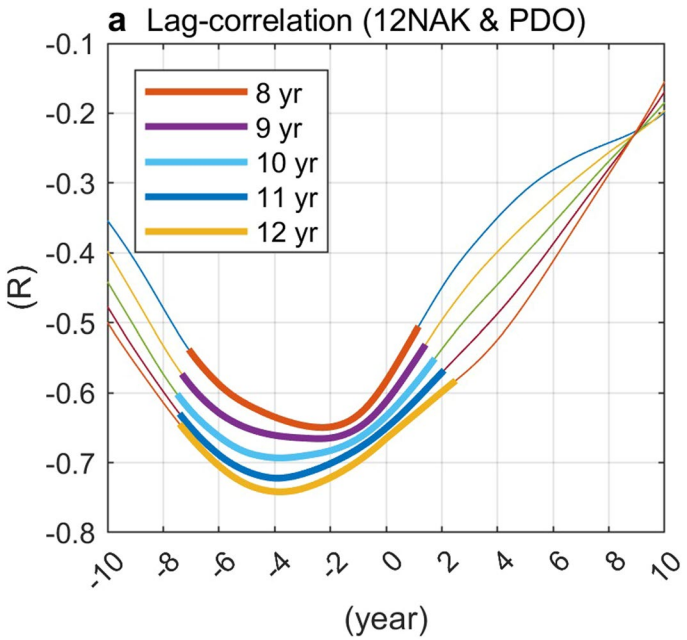

Extended Data Fig. 5 | Lag correlation between the Solomon Sea CS-δ^{15}N and the PDO. The Solomon Sea CS-δ^{15}N is best correlated with the PDO with a 2–4 years lag time. Different colors represent results when applying different number of years for running mean, which appears to have small effect for calculating the lag correlation.

https://doi.org/10.1038/s41561-023-01212-4

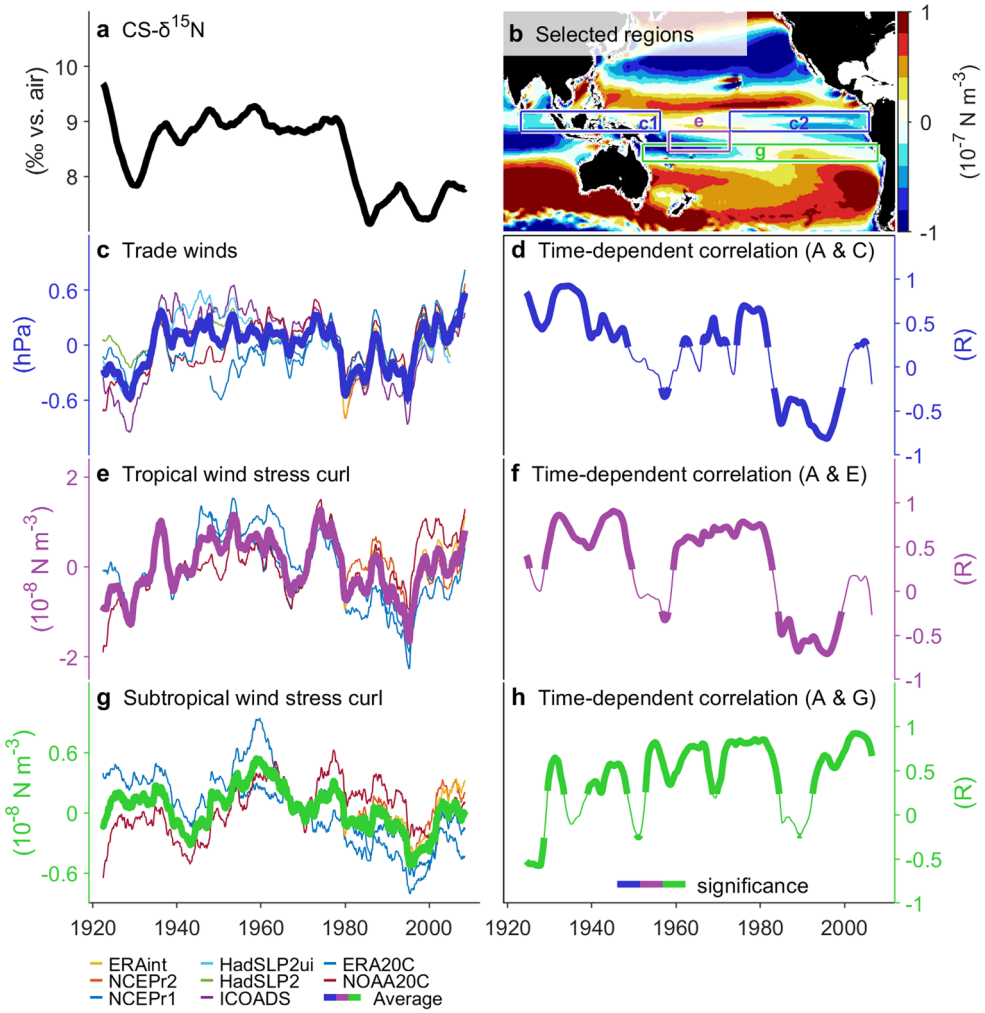

Extended Data Fig. 6 | Correlation between CS-δ^{15}N and tropical *vs.* subtropical winds. a, 7-year running mean of the Solomon Sea CS-δ^{15}N. **b**, Wind stress curl difference (color, in 10^{-7} N m^{-3}) between 1960–1980 (negative PDO phase) and 1980–2000 (positive PDO phase). Boxes indicate regions where tropical and subtropical winds are computed from data reanalysis product[58,68–73]. The strength of the equatorial trade winds in **c** is computed from a large-scale tropical SLP gradient (ΔSLP) between the central/east Pacific (160°W–80°W) and the west Pacific/Indian Ocean (80°E–160°E) (box c2 and c1). The index is computed with SLP anomalies from monthly climatology and averaged over grid cells within 5° latitude of the equator, then averaged with 7 years window. The tropical and subtropical wind stress curl anomalies in panel **e** and **g** are computed from monthly climatology and averaged over the area in box e (5°S-15°S, 165°E-160°W) and in box g (11.5°S-20°S, 150°E-75°W) respectively, then averaged with 7 years window. During positive PDO phase between 1980 and 2000, the trade winds weaken, and the wind stress curl in the tropical and subtropical bands both show a negative anomaly. The decadal changes in the CS-δ^{15}N are significantly correlated with changes in the wind at a period of 11 years, but the CS-δ^{15}N showed a delayed response from changes in the equatorial trade winds and tropical wind stress curl. Specifically, the CS-δ^{15}N changes are largely in phase with changes in the wind stress curl, but were out of phase after the 1980s. But the decadal changes in the CS-δ^{15}N are significantly correlated with and are largely in phase with changes in the wind stress curl in the subtropical South Pacific. In **d**, **f**, and **h**, the thick lines indicate periods when CS-δ^{15}N is significantly correlated with the wind changes with 99% confidence level.

https://doi.org/10.1038/s41561-023-01212-4

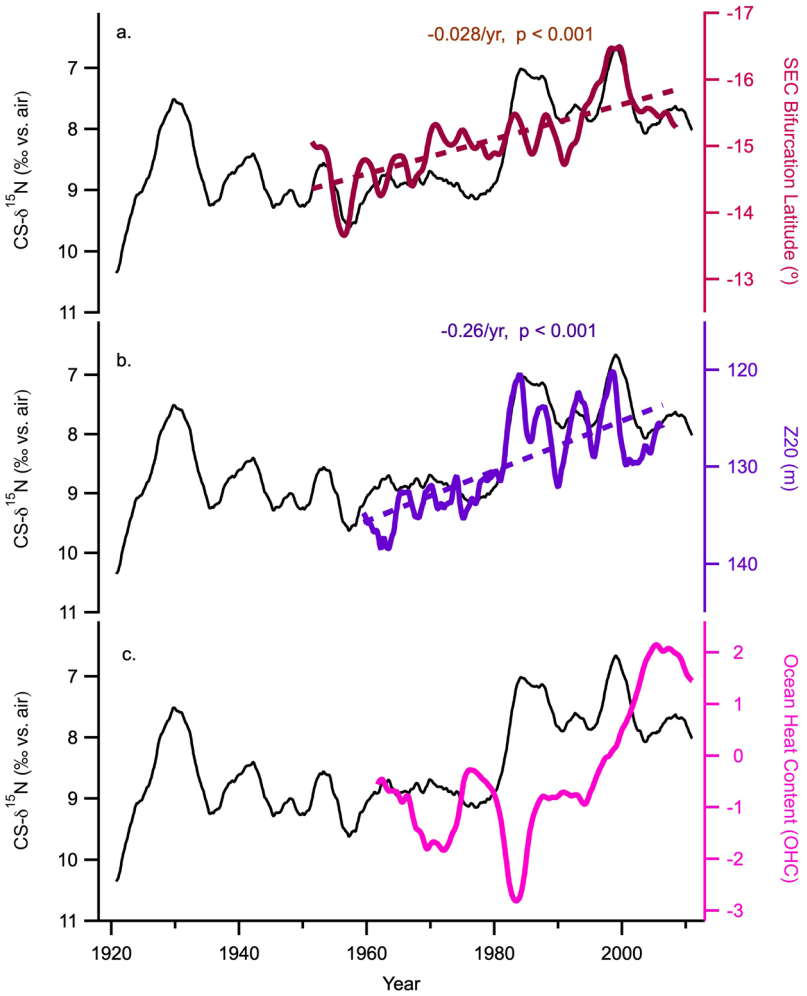

Extended Data Fig. 7 | CS-δ^{15}N changes in comparison with bifurcation latitude of the SEC, the mean equatorial thermocline depth and the ocean heat content in the tropical/subtropical Pacific. a, The decadal and long-term decreasing trend in the CS-δ^{15}N are accompanied by changes in the bifurcation latitude of the SEC[41]. Southward migration of the SEC bifurcation latitude results in more equatorward transport into the Solomon Sea[18,74], contributing to decrease in the CS-δ^{15}N. The detrended changes in CS-δ^{15}N are also significantly correlated with changes in the bifurcation latitude (r = 0.38, p = 0.09; 3-year running average). **b**, The declining trend in CS-δ^{15}N is accompanied by long-term shoaling of the mean thermocline depth in the equatorial Pacific. The thermocline depth in the equatorial Pacific is defined as the depth of the 20 °C isotherm (Z_{20};[75]), and is calculated from the global ocean based on the Simple Ocean Data Assimilation (SODA, version 2.1.6) package[76] for the equatorial Pacific basin mean (5°S-5°N, 130°E-80°W)[77]. The detrended changes in CS-δ^{15}N are also significantly correlated with Z_{20} (r = 0.67, p = 0.01; 3-year running average). **c**, Decrease in the CS-δ^{15}N, thus increase in the western boundary current transport, appears to coincide with decrease in the ocean heat content in the upper 700 m in the tropical/subtropical Pacific[78]. This supports the importance of the STCs in contributing to the heat recharge-discharge dynamics on interannual/decadal time scales[13]. All data are smoothed by 3-yr running mean.

https://doi.org/10.1038/s41561-023-01212-4

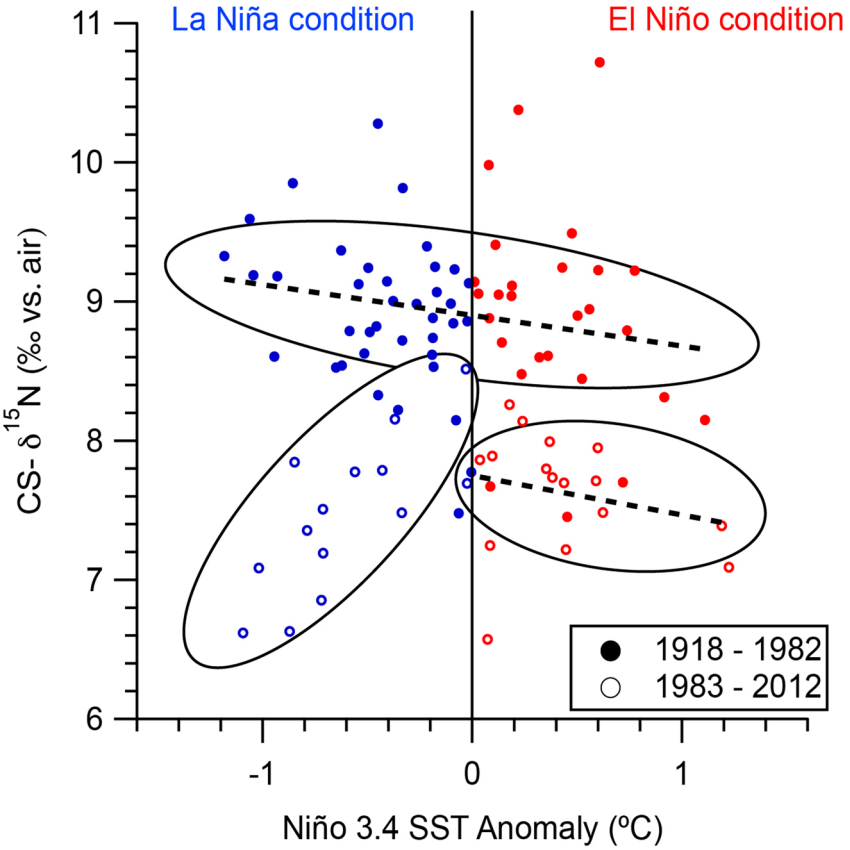

Extended Data Fig. 8 | Cross-comparison between the annual averages of CS-δ^{15}N and Niño 3.4 index. The CS-δ^{15}N is generally negatively correlated with Niño 3.4 SST anomalies[66], with lower values during El Niño conditions. However, the relationship breaks down after 1982, largely because that CS-δ^{15}N no longer increases during La Niña conditions.